**Amorphous to Nanocrystalline Alloys for Soft Magnetic Applications**

Matthew A. Willard and Vincent G. Harris

Materials Physics Branch, Code 6340, Naval Research Laboratory, Washington, D.C.

## Introduction

The development during the late 1970's of amorphous metal alloys, consisting primarily of ferromagnetic transition metals (Fe, Co, Ni or combinations thereof), led to their commercialization of ultrasoft magnetic materials for a myriad of applications in power conversion, conditioning and generation [1].

The advantages of an amorphous local structure were primarily seen in the reduction of magnetic anisotropy [2] and the corresponding improvement in such related properties as hysteresis and permeability. In addition, the frustrated atomic structure led to values of electrical resistivity ($\rho \geq 100$ μΩ-cm) many times greater than those of metallic alloys, thus allowing for higher frequency operation. Disadvantages intrinsic to the metallic glasses include the dilution of magnetization (also saturation induction) relative to the all-metal alternatives from the necessity to include glass stabilizing elements, and costly processing.

Notwithstanding these detractors, metallic glasses defined a niche market for inductor applications in the 10 kHz $\leq f \leq$ 100 kHz frequency band as well as for a broad range of sensor applications. In developing countries such as India and China, who were, and continue to construct their modern power grids, metallic glasses have found wide use as cores in distribution transformers.

In 1988, Y. Yoshizawa, S. Oguma, and K. Yamauchi [3], developed a nanocrystalline variant of these metallic glasses. Their alloy, $Fe_{0.735}Si_{0.135}B_{0.09}Nb_{0.03}Cu_{0.01}$, differs from conventional metallic glasses by the addition of small amounts of Nb and Cu. This alloy has since been trademarked and is known as Finemet™. These dilute additives play a large role in the crystallization kinetics and the stability of the nanocrystalline structure. In contrast to metallic glasses, a crystallization heat treatment leads to a morphology that has Fe-Si ($DO_3$) grains approximately 10-12 nm in diameter embedded within an amorphous matrix. This nanocrystalline composite structure is remarkably stable in temperature against grain growth allowing for design engineers to contemplate high temperature applications.

**Alloy Design and Processing**

Since magnetic domain walls move through a material as its magnetization is swept from the top of one cycle to the bottom of the next, the 'pinning' or hindrance of these walls lead to high-loss behavior in inductor applications. As such, one might expect that nanocrystalline materials having copious grain boundaries (e.g. domain wall 'pinning' centers) would be characterized as being 'lossy.' A random anisotropy model, originally developed for amorphous alloys, explains this seemingly anomalous behavior. The application of this model to nanocrystalline alloys shows that as the grain diameter is reduced below the exchange correlation length, the magnetocrystalline anisotropy energy is averaged over the exchange volume resulting in very small values [4]. This in turn allows for the domain wall to pass unimpeded through the material.

Therefore, although conventional alloy design requires an increase in grain size to reduce the coercivity by reducing the grain boundary density, the design of

nanocrystalline alloys *requires* the grains to be small in comparison to the magnetic exchange length. Using this philosophy, additional alloys have been developed with increased magnetization (e.g. Nanoperm™[5]) and high Curie temperatures (e.g. HiTperm[6]). Some of these are listed in Table I with their magnetic properties and targeted applications.

*Design*

Amorphous alloys are thermodynamically metastable, therefore, the formation of these materials require non-equilibrium processing. The most widely used technique for the synthesis of amorphous alloys is the melt spinning process, where a molten metal alloy is ejected through an orifice onto a rotating copper wheel. This provides a $10^5$-$10^7$ °C/s quench rate sufficient to freeze the alloy as a glass and avoid nucleation and growth of crystallites. The form of processing produces a wide (~20 mm) and thin (~30 μm) ribbon that can readily be spun as a toroid.

Only compositions that are close to deep eutectics will allow the glass to form at these quench rates. The magnetization of the alloy is directly related to the amount of magnetic transition metal (i.e. T = Fe, Co, Ni). The relative fraction of these are maximized in the alloy design that must also contain metalloid elements (i.e. M = B, Si, P, C, etc.) in order to stabilize the glassy phase. In traditional metallic glasses the ratio of T:M is 8:2. The early transition metal elements (i.e. Zr, Nb, Hf, etc.) provide a similar glass stabilizing function with the added feature that they inhibit diffusion in these alloys. Since the eutectic that exists in T-Zr binary phases occurs near T~88%, the use of these elements allow for a greater fraction of T and subsequently a higher magnetization. This

obvious advantage is somewhat offset by the cost of these elements and their reactivity that leads to greater degradation via oxidation.

*Processing*

Both amorphous and nanocrystalline alloys rely on the formation of amorphous ribbons by melt spinning as a preliminary step. In addition to choosing compositions near deep eutectics, the superheat of the melt, the crucible orifice size, the wheel speed, and the pressure of ejection gas all play a role in determining the morphology of the resulting ribbons. Annealing in an applied magnetic field is used to tailor the permeability of amorphous ribbons for specific applications. For nanocrystalline alloys, an optimal heat treatment is needed to obtain the desired nanocrystalline structure. A magnetic field annealing may also be shown effective in the tailoring of permeability for these alloys.

**Structure and Magnetism**

*Structural Properties*

The development of nanocrystalline alloys relies on the diffusion barrier provided by the early transition metals to inhibit grain growth. This is apparent in Figure 1, where two sets of Finemet-based alloys are examined by transmission electron microscopy. The Finemet material is amorphous in the as spun state (Fig. 1(a)). After annealing, at 550 °C for as much as 7200 s, the grain size remains below 10 nm (Fig. 1(b-c)). When Nb is replaced by Fe in these alloys, the diffusion barrier is omitted and grain growth occurs upon heating, growing to 50 nm in just 3600 s (Fig. 1(d-f)).

In 1998, Ayers et al. [10] proposed the now accepted model of the crystallization kinetics of Finemet™. This model describes the early precipitation of Cu as fcc

nanoclusters that act as nucleation sites for the crystallization of $DO_3$ FeSi crystals. As the $DO_3$ FeSi crystals grow the nearby amorphous phase is depleted in Fe and becomes richer in Nb. The Nb functions as a glass stabilizer and is effective in limiting the growth of the $DO_3$ crystallites. Nb may also play a role in limiting the solubility of Cu in the amorphous phase.

To determine the optimal annealing temperature, the as-spun ribbon is examined by differential scanning calorimetry to identify the primary and secondary crystallization temperatures, $T_{x1}$ and $T_{x2}$, respectively. It is imperative that the first phase to crystallize be the ferromagnetic phase giving rise to a high magnetization in the crystallized alloy. Additionally, an appreciable difference between $T_{x1}$ and $T_{x2}$ is necessary so that the deleterious affects of secondary phase formation are avoided. Figure 2 shows the exothermic crystallization peaks for Finemet™-type alloys, with and without 3 at% Nb.

*Magnetic Properties*

Figure 3 is a plot of hystersis loops (M vs H) for FeNiZrB alloys and are representative of the nanocrystalline soft magnetic alloys in the as-spun, optimally annealed (between $T_{x1}$ and $T_{x2}$), and over annealed (above $T_{x1}$ and $T_{x2}$) states. Upon optimal annealing crystallization, the magnetization rises while the coercivity increases slightly due to the increased magnetocrystalline anisotropy of the crystallites. This contrasts the significant increases in the coercivity, lowering of saturation magnetization and changed loop shape found in the samples annealed at temperatures above $T_{x2}$. The increased coercivity comes from the increased grain size of the nanocrystallites, the formation of secondary phases consisting of borides and magnetic transition metal/early transition metal intermetallics with higher magnetocrystalline anisotropies, and the

secondary phases acting as domain wall pinning sites. The loop shape change from a single shoulder loop to one with two shoulders in the second quadrant is indicative of the weakened exchange coupling between the two phases.

**What the Future Holds**

Nanocrystalline soft magnetic alloys have evolved from metallic glasses. While the alloy compositions for nanocrystalline materials have been necessarily modified from amorphous alloys to inhibit diffusion, the same basic melt spinning technique has been implemented. Favorable magnetic properties have been demonstrated for the nanocrystalline materials with improved properties over existing amorphous and conventional “large-grained” magnets. Future progress will undoubtedly include improvements in lower magnetostriction and increased exchange coupling in the residual amorphous phases.

**Acknowledgement**

This work was funded in part under grants from the Office Naval Research and Air Force Research Office. The authors gratefully acknowledge the assistance of Mr. Harry Jones and Dr. James Sprague for sample processing and TEM, respectively.

**References**


1. R. C. O' Handley. *J. Appl. Phys.* **62** (1987) R15-49.
2. Magnetic anisotropy is a term used to describe a sample's internal energy as a function of magnetization direction.
3. Y. Yoshizawa, S. Oguma, and K. Yamauchi. *J. Appl. Phys.* **64(10)** (1988) 6044-47.
4. G. Herzer, *IEEE Trans. Mag.* **26(5)** (1990) 1397-1402.
5. K. Suzuki, N. Kataoka, A. Inoue, A. Makino, and T. Masumoto. *Mat. Trans. JIM* **31** (1990) 743-46.
6. M. A. Willard, D. E. Laughlin, M. E. McHenry, D. Thoma, K. Sickafus, J. O. Cross, and V. G. Harris. *J. Appl. Phys.* **84** (1998) 6773-77.
7. M. E. McHenry, M. A. Willard, and D. E. Laughlin. *Prog. Mat. Sci.* **44(4)** (1999) 291-433.
8. http://www.electronicmaterials.com/businesses/sem/amorph/index.html
9. http://www.hitachi-metals.co.jp/english/cat/pdf/e22b.pdf
10. J. D. Ayers, V. G. Harris, J. A. Sprague, W. T. Elam, and H. N. Jones. *Acta Mater.* **46(6)** (1998) 1861-1874.
11. M. A. Willard, J. H. Claassen, and V. G. Harris. *Proc. First IEEE Conference on Nanotechnology* (2001) 51-55.

**Biography**

Matthew A. Willard received his Ph.D. in Materials Science and Engineering from Carnegie Mellon University in 2000. He is currently a NRC postdoctoral associate at the U.S. Naval Research Laboratory.

Vincent G. Harris is the head of the Materials Physics Branch at the U.S. Naval Research Laboratory. He received his Ph.D. from Northeastern University in 1990.

**Table 1: Properties and Applications of Metglas™, Finemet™, Nanoperm™, and HiTperm Alloys[7-9]**

| Alloy | Magnetic Phase | $\mu_0 M_s$ (T) | $\mu$ | $H_c$ (A/m) | Application |
|---|---|---|---|---|---|
| Finemet | $DO_3$-(Fe,Si) + Amorphous | 1.23-1.35 | 5k-100k | 0.6-3.1 | Transformers, Filters, Choke Coils |
| Nanoperm | α-Fe + Amorphous | 1.52-1.64 | 3.5k-48k | 2.4-4.5 | Transformers, Filters |
| Hitperm | α'-FeCo + Amorphous | 1.6-1.9 | 1k-5k | 80-200 | High Temperature Cores |
| Metglas® 2605CO | Fe-based Amorphous | 1.8 | 120k-400k | 4 | Cores, Sensors |
| Metglas® 2714A | Co-based Amorphous | 0.57 | 80k-1000k | 0.3 | Transformer, Sensors |
| Metglas® 2705M | Co-based Amorphous | 0.77 | 290k-600k | 1.2 | Cores, Sensors |
| Metglas® 2826MB | Fe-Ni-based Amorphous | 0.88 | 50k-800k | 10 | Cores, Sensors |

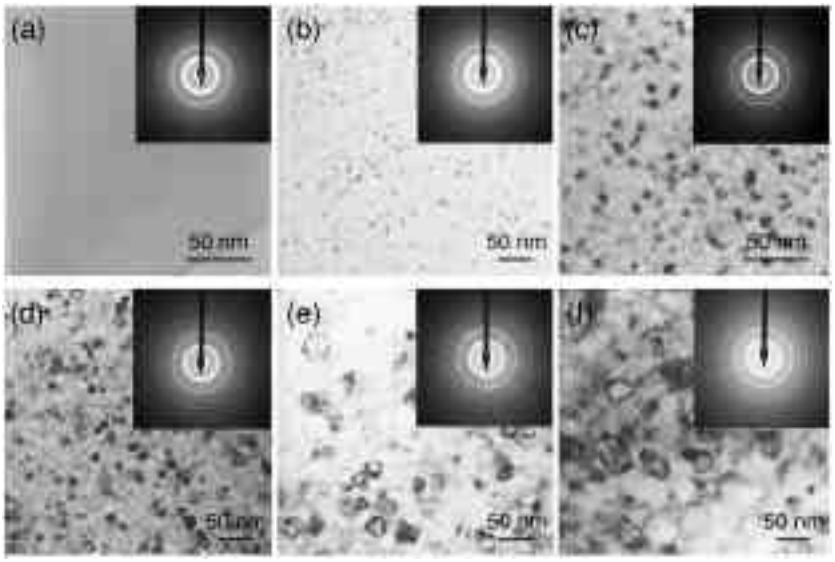


Figure 1: Transmission electron microscopy images of the standard Finemet™ alloy ($Fe_{0.735}Si_{0.135}B_{0.09}Nb_{0.03}Cu_{0.01}$): (a) as spun (b) 120 s at 550 °C (c) 7200 s at 550 °C; Finemet™ alloy without Nb ($Fe_{0.765}Si_{0.135}B_{0.09}Cu_{0.01}$): (d) 8 s at 550 °C (e) 120 s at 550 °C (f) 3600 s at 550 °C

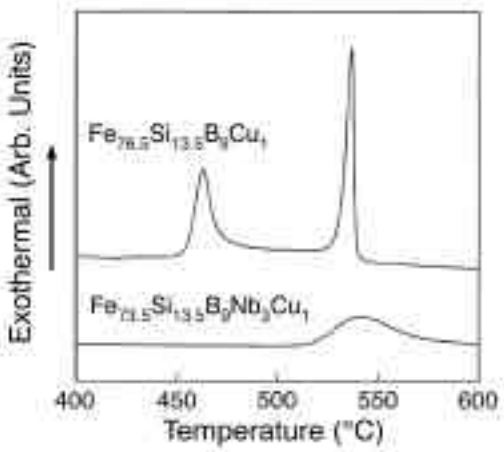


Figure 2: Differential scanning calorimetry data for $Fe_{73.5-x}Si_{13.5}B_9Nb_xCu_1$ alloys[10]

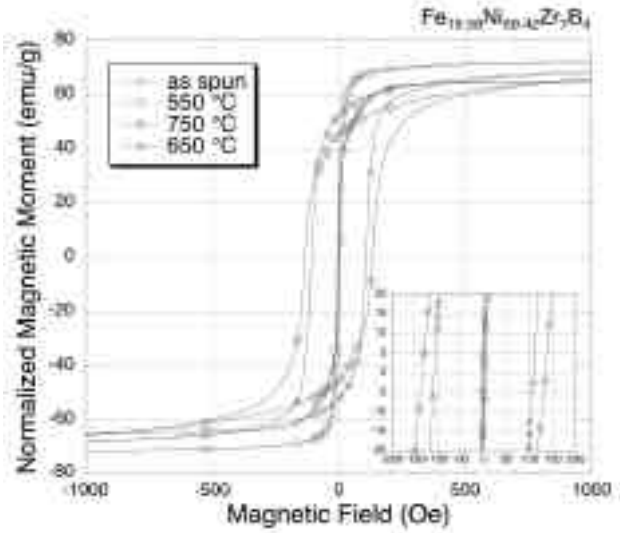


Figure 3: Typical DC hysteresis loops of the as-spun precursor alloy, nanocrystalline alloy with optimal anneal (550 °C) and excessive annealing temperatures (650 and 750 °C).[11]